Molecular Dynamics Simulation of a Perylene-Derivative Langmuir Film

André F. de Moura and Milan Trsic*

Departamento de Química e Física Molecular, Instituto de Química de São Carlos, Universidade de São Paulo, CP 780, 13560-970 São Carlos, SP, Brazil

Received: October 15, 2004; In Final Form: December 22, 2004

We performed a series of molecular dynamics simulations of an *N*,*N*′-di-*n*-butyl-3,4:9,10-perylene tetracarboxydiimide (BuPTCD) Langmuir film. The film was studied at three surface areas (0.38, 0.40, and 0.45 nm^2 $molecule^{-1}$) using model systems consisting of one BuPTCD monolayer on each side of a 6.0-nm-thick water slab. On the basis of geometrical reasoning and surface pressure results, it was found that perylene molecules seem to be oriented mainly head-on toward the water surface. On the other hand, the average orientation of the perylene tetracarboxidiimide moiety during simulations indicated that molecular alignment is not simple, changing from tilted face-on to tilted head-on during compression. The change in orientation of BuPTCD molecules was accompanied by the thickening of the film as the area decreased. Films also became more orderly at small surface areas, mostly at the rigid perylene core. BuPTCD molecules are not evenly hydrated, with very few solvent molecules hydrating the hydrophobic tails, whereas a considerable number of water molecules were hydrogen bonded to diimide oxygen atoms. Besides, the residence times of water molecules around perylene atomic sites increased from the terminal methyl groups to the diimide oxygen atoms. Finally, the electric potential profile across the monolayer was found to depend on the area occupied by each molecule, indicating that properties of the films may vary considerably with the area occupied by each molecule. Altogether, the molecular description arising from our computer simulations suggests which structural patterns may be found in these films depending on the surface density of perylene molecules.

1. Introduction

1.1. Perylene-Derivative Structures and Applications. Perylene tetracarboxidiimide derivatives (PTCD) are dyes mostly used in car painting. These organic semiconductor compounds have received attention in recent years as candidate molecules to build optoelectronic devices (e.g., organic solar cells,[1,2] xerographic applications,[3] and dye lasers).[4] PTCD thin films have been used to construct solar cells on the basis of p−n junctions, whose efficiency depends strongly on molecular ordering into each monolayer, but so far they are not as efficient as inorganic devices.[1,2,5−7]

The electronic structure of a perylene molecule is determined mostly by its aromatic moiety,[8] but the molecular order plays an important role in the electronic properties of PTCD in condensed phases. Changes in absorption spectra due to molecular packing in different crystals were reported for several compounds,[9−11] an effect known as crystallochromy. It may seem quite obvious that different substituents attached to the aromatic moiety should change solid-state spectra, but Mizugushi[12] showed that the crystal color may be different even for the same compound, depending on the way the crystals were grown. He crystallized *N*,*N*′-di-*n*-butyl-3,4:9,10-perylene tetracarboxydiimide (BuPTCD) from its vapor and obtained black needle crystals, in contrast with the red-maroon crystals previously reported by Hädicke and Graser.[9] The latter were recrystallized from nitrobenzene and presented only one molecule per unit cell, while the former had two molecules per unit cell with a different conformation for the aliphatic chains. Interestingly, both crystals have the same density; that is, the difference in the molecular packing is subtle enough not to produce a significant change in density but has a marked influence on the spectroscopic properties.

Klebe et al.[11] found a correlation between the absorption spectra and the crystallographic parameters of perylene derivatives. They derived an empirical equation relating the maximum absorption wavelength to the longitudinal and transversal displacements of two neighboring perylene molecules. Kazmaier and Hoffmann[13] used an extended Hückel method to show that the spectra did not vary because of the extent of area superposition of two adjacent molecules; instead, they showed that the variation was due mainly to quantum interference effects in the frontier orbitals.

Optoelectronic applications usually employ PTCD thin films, which may be prepared using several techniques (e.g., Langmuir−Blodgett, spin coating, or vacuum evaporation). Liu et al.[14] reported changes in the colors of liquid-crystal perylene films upon aging, showing that these films also presented crystallochromy. The same work[14] presented X-ray diffraction patterns, showing that colors were related to changes in molecular ordering and were not dependent on the substrate employed or on the deposition method.

The Langmuir−Blodgett technique consists of the transfer of a Langmuir film from an aqueous subphase to any suitable solid substrate. In the present work, we shall be concerned with the description of BuPTCD Langmuir films using molecular dynamics simulations. In the next section, we shall give a brief account of previously reported theoretical studies of Langmuir films.

1.2. Theoretical Studies of Langmuir Films. Langmuir films are obtained when an amphiphilic or hydrophobic substance spreads on the air/water interface.[15,16] The early studies about

* Corresponding author. E-mail: milan@iqsc.usp.br. Phone: 55-16-3373-8032. Fax: 55-16-3373-9975.

10.1021/jp0452711 CCC: $30.25
Published on Web 02/09/2005

these films gave some of the first evidences regarding the size of molecules, even before their existence was widely accepted.

Several techniques have been used to characterize Langmuir films, especially the determination of surface pressure versus area per molecule isotherms.[16] Different phases may be assigned to regions comprising an isotherm, each having a different molecular packing and orientation. At a very high area per molecule, the film is said to be a two-dimensional gas (phase G). Upon compression, this phase changes to more orderly structures until a critical pressure is achieved and the film collapses into, for example, multilayers or aggregates.

Phase transitions are characterized by changes in the orientation of molecules comprising the film. Iwamoto et al.[17] have proposed a theoretical model to account for the transitions between the smectic A and tilted smectic C phases of liquid-crystal thin films. According to their model, steric repulsion tends to align molecules with their principal axis perpendicular to the interface, whereas dipole interactions tend to tilt their principal axis away from this orientation. The competition between these two factors would be responsible for the different structural patterns observed.

Computer simulations may provide a means to understand Langmuir monolayers at the molecular level. Early simulations employed simplified model systems, composed of pseudoatoms to represent lipid molecules and an effective interaction to mimic the headgroup-water potential.[18−21] These works focused on the dependence of chain structure and dynamics on the area per molecule[18−20] and the coexistence region of liquid-expanded (LE) and liquid-condensed (LC) phases.[21] At the same time, Ahlström and Berendsen[22] reported a series of molecular dynamics simulations of lecithin monolayers at the air/water interface with an area per molecule corresponding to the LE phase. Their model system still employed pseudoatoms to describe lipid molecules but included explicit water molecules. They compared three different force fields for the lipid molecules and found good agreement with the experimentally determined surface pressures for all of them, showing the feasibility of carrying out detailed computer simulations to describe structural and dynamic properties of Langmuir films.

Other molecular dynamics simulations of Langmuir films have been reported, including those of decyl-β-glucoside and dilauroyl-*sn*-glycerol,[23] stearic acid,[24] sodium laurate,[25] (octadecylamino)dihydroxysalicylaldehyde,[26] and zwitterionic lipids using both atomistic[27−29] and coarse-grain models.[30] Okamura et al.[24] calculated the infrared spectra of stearic acid as a function of the area per molecule and showed that methylene stretching modes were shifted during compression while carbonyl modes were not. Dhathathreyan and Collins[26] reported a steep increase in the total pressure of (octadecylamino)dihydroxysalicylaldehyde below 0.24 nm^2 molecule^{-1}, indicating a possible transition from the G to LE phase. Nielsen et al.[30] performed a series of molecular dynamics simulations of zwitterionic lipids using coarse-grain models and found two possible mechanisms to release excess pressure from metastable monolayers at high surface coverage, either by means of a surface curvature or by moving some headgroups away from the monolayer.

In the present paper, we report the results obtained from a series of molecular dynamics simulations of BuPTCD Langmuir films. To the best of our knowledge, these are the first simulations of semiconductor thin films using an atomistic model. As we pointed out, molecular order plays a central role in determining the electronic properties of PTCD thin films,[5−7] so we aim to improve the understanding of the ordering of BuPTCD molecules at different surface densities as well as their hydration.

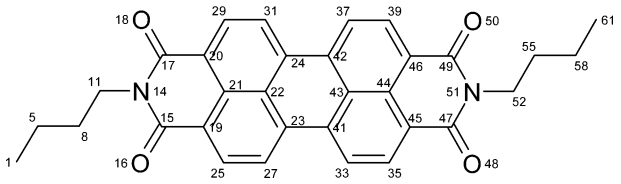

Figure 1. BuPTCD structure and atom numbering. Only heavy atoms are shown; hydrogen numbers follow the numbering of the heavy atom they are bonded to.

2. Methodology

It is well-known that complex liquid systems are characterized by hierarchical relaxation times spanning several orders of magnitude, so we cannot ever hope to sample their whole phase space in any simulation approach to the statistical mechanical problem. Nonetheless, molecular dynamics simulations have been successfully employed to describe phenomena that relax within the duration of a typical run.[31] Shinoda et al.[32] showed that lipid bilayers that had been assembled in different ways attained the same average structure in ca. 0.5 ns. Paci and Marchi[33] studied the adequacy of two pressure coupling schemes usually employed in molecular dynamics simulations and found that the volume of water/protein systems relaxed within tens of picoseconds after sudden pressure jumps were applied. In recent years, the self-assembling of micelles[34,35] and bilayers[36] in aqueous solutions has been reported, showing that it is now feasible to treat complex systems using atomic-detail simulations to obtain reliable structural parameters. In this section, we shall describe the methodology and the model systems that were employed in a series of molecular dynamics simulations of BuPTCD Langmuir films.

2.1. Interaction Parameters. The water-molecule potential surface was described by the solid phase crystallization (SPC) model.[37] BuPTCD interaction parameters were taken mostly from the OPLS-AA force field,[38] except for the atomic charges of the perylene moiety, which were derived using the restrained electrostatic potential (RESP) methodology,[39−40] constraining only the methyl and the next two methylene groups to have their standard OPLS-AA charges. A RHF/6-31g*//AM1 single-point calculation was carried out to generate BuPTCD's electrostatic potential using the Gaussian 03 program.[41] The ab initio calculation and the charge fitting were performed using the graphical interface of the XRED program,[42] making the whole process straightforward. We present the BuPTCD structure and atom numbering in Figure 1 and partial atomic charges in Table 1.

2.2. Langmuir Films Assembling. A stable LC phase is observed down to 0.38 nm^2 molecule^{-1} during the first compression of BuPTCD Langmuir films.[43] The surface pressure decreases during the second compression but changes little during the third one, possibly because of the formation of stable molecular aggregates. During the second and third compressions, the surface pressure becomes greater than zero only below 0.45 nm^2 molecule^{-1}, so we have chosen to model BuPTCD films between 0.38 and 0.45 nm^2 molecule^{-1}.

Complex liquids do not relax in the course of a typical molecular dynamics run, so it is necessary to input some structural information in the starting configurations.[44] To avoid memory effects due to this a priori information, it is also necessary to check whether different initial structures will evolve

TABLE 1: BuPTCD Atomic Charges Derived Using RESP Methodology

atom number	partial charge (*e*)
1, 61	−0.180[a]
5, 8, 55, 58	−0.120[a]
2−4, 6, 7, 9, 10, 56, 57, 59, 60, 62−64	0.060[a]
11, 52	0.105
12, 13, 53, 54	0.030
14, 51	−0.165
15, 17, 47, 49	0.510
16, 18, 48, 50	−0.510
19, 20, 45, 46	−0.075
21, 44	0.000
22−24, 41−43	0.050
25, 29, 35, 39	−0.195
26, 30, 36, 40	0.195
27, 31, 33, 37	−0.165
28, 32, 34, 38	0.165

[a] Standard OPLS-AA parameters.

into similar final structures. In the case of perylene-derivative thin films, three molecular orientations are postulated: face-on, edge-on, and head-on (Figure 2). Experimental investigations pointed to the head-on as the most probable orientation for several PTCD derivatives.[43,45,46] We aim to find out which of them may actually occur in BuPTCD Langmuir films, but it is not likely that one orientation will change into another during simulation. For this reason, three model systems need to be assembled, one for each possible orientation.

Each perylene film was initially composed of 120 BuPTCD molecules, arranged in such a way as to yield an area of around 0.38 nm^2 molecule^{-1}. For the face-on orientation, BuPTCD molecules were assembled in a rectangular array with 4 × 6 × 5 molecules in the *x*, *y*, and *z* directions, respectively. For the edge-on orientation, a rectangular array with 4 × 15 × 2 molecules was chosen. Also, for the head-on orientation, an array with 20 × 6 × 1 molecules was employed. These structures were optimized using 5000 steps of the L-BFGS algorithm[47] to avoid strong repulsive contacts between BuPTCD molecules, followed by simulated annealing cycles until the potential energy and the box size became stable. The annealing was performed using weak coupling to heat and pressure baths[48] ($\tau_T = 0.1$ ps; $\tau_p = 1.0$ ps; $p = 1$ bar), varying the temperature cyclically between 300 and 400 K every 20 ps. Pressure coupling was semi-isotropic, allowing box edges to relax independently while keeping the rectangular shape. The model systems were further equilibrated during a 20 ps run using the constant-NVT ensemble (canonical ensemble) at 288 K ($\tau_T = 0.1$ ps), the same temperature employed to determine the experimental surface pressure isotherms.[43] After equilibration was complete, each system was replicated along the *z* axis, the two replicas being separated by 6.0 nm. This empty space was then filled with SPC water molecules at random positions, and the box edge along the *z* direction was set to 50.0 nm, resulting in one BuPTCD film on each water/air interface. As a final preparation step, BuPTCD molecules were randomly removed from each film to achieve an area equal to 0.38, 0.40, or 0.45 nm^2 molecule^{-1}, and the potential energy was minimized with 100 steps of the L-BFGS algorithm.

2.3. Simulation Details. Trajectories were run up to 1 ns with a time step of 1 fs without any geometry constraint. The NVT ensemble was employed, coupling each film and the water subphase to a different temperature bath ($T = 288$ K; $\tau_T = 0.1$ ps). Nonbonded interactions were truncated using a 0.8/1.4 nm twin-range cutoff for Lennard-Jones and Coulomb interactions, respectively. Dispersion correction was applied to the energy, and the neighbors list was updated every fifth step. All analyses were performed using the last 500 ps of data, using coordinates recorded at 0.5 ps intervals and energy at 0.05 ps intervals. All simulations were carried out using the GROMACS 3.2.1 package[49,50] on a 2.8 GHz P4 computer running the RedHat Linux operational system (version 9.0).

3. Results and Discussion

3.1. Surface Pressure Isotherms. The molecular packing obtained during the assembling process described above showed that only the head-on orientation could form a true monolayer with an area as low as 0.38 nm^2 molecule^{-1}, the other two orientations reaching such a small area only if two or more BuPTCD layers were stacked (Figure 3).

Besides this geometrical reasoning about the possible molecular packing of BuPTCD Langmuir films, the surface tension may be readily derived from molecular dynamics simulations, from which the surface pressure may be calculated and compared with experimental data. The instantaneous surface pressure (π) is defined as

$$\pi = \gamma_0 - \gamma$$

where γ_0 is the water surface tension and γ is the surface tension of the system. The surface tension may be derived from the difference of pressure between the direction perpendicular to the interface and the parallel directions

$$\gamma = \frac{L_z}{2}\left[p_{zz} - \frac{p_{xx} + p_{yy}}{2}\right]$$

where L_z is the dimension of the box in the *z* direction and p_{xx}, p_{yy}, and p_{zz} are the diagonal elements of the pressure tensor.

Experimentally determined BuPTCD isotherms at 288 K show a significant decrease in the surface pressure in the second compression of the film in comparison with that of the first one.[43] Only minor changes were observed in the surface pressure between the second and third compressions of the film. The authors in ref 43 attributed this behavior to the formation of stable aggregates, although there is no direct experimental evidence showing what the intermolecular arrangement in these Langmuir films should be.

The calculated surface pressures for the head-on orientation at 0.40 nm^2 molecule^{-1} agreed reasonably well with experimental values for the first compression of the BuPTCD film while the other two orientations resulted in negative surface pressures (Table 2). The negative values indicate that these multilayer arrangements are metastable and would need much longer simulation times to achieve true equilibrium. Although the systems with edge-on and face-on orientations did not attain equilibrium within the duration of the trajectories, our results suggest that head-on is the preferred molecular orientation during the first compression because it can yield a true monomolecular film and a surface pressure in good agreement with the experimental value. In the following discussions, only the head-on orientation will be dealt with.

Experimentally, there is a collapse point in any surface-pressure isotherm, characterized as the limiting area below which the surface pressure starts to decrease upon further compression. The surface pressure decrease is possibly due to the formation of multilayered structures, which are not closely packed and may be further compressed without a corresponding increase in the surface pressure. For BuPTCD at 288 K,[43] the collapse takes place at 0.38 nm^2 molecule^{-1}. Our theoretical results show the opposite trend; the surface pressure increased as the

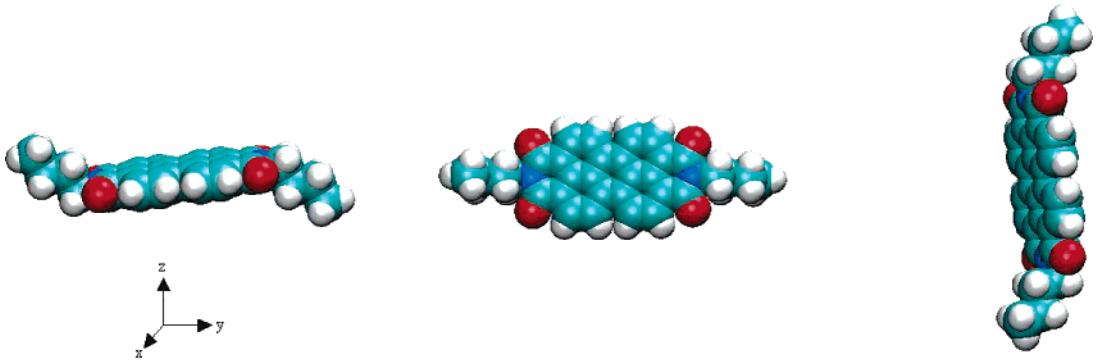

Figure 2. BuPTCD orientation with respect to the water surface at the $x-y$ plane: face-on, edge-on, and head-on orientations (from left to right).

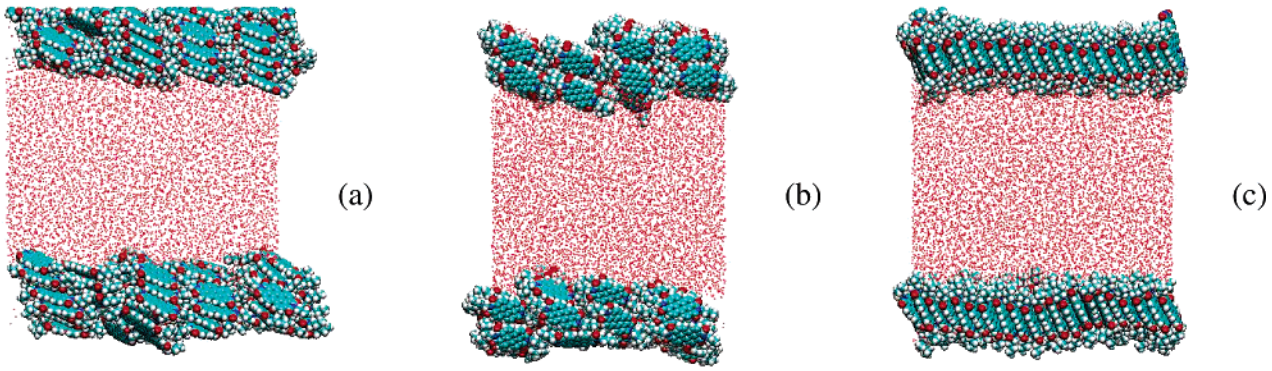

Figure 3. BuPTCD films on water after 1 ns at 0.40 nm^2 molecule^{-1}: (a) face-on; (b) edge-on; (c) head-on.

TABLE 2: BuPTCD Film Surface Pressure (T = 288 K)[a]

area (nm^2 molecule^{-1})	orientation	surface pressure (mN m^{-1})
0.38	head-on	110
	experimental (first compression)	49
	experimental (second compression)	6.5
0.40	face-on	−37
	edge-on	−43
	head-on	48
	experimental (first compression)	44
	experimental (second compression)	4.5
0.45	head-on	−41
	experimental (first compression)	27
	experimental (second compression)	0

[a] Experimental data were taken from Constantino et al.[34]

molecular area changed from 0.40 to 0.38 nm^2 molecule^{-1} (Table 2). This apparent contradiction is possibly due to the long time required to collapse such an orderly film as compared to the time scale within reach at the present time for computer simulations. Nevertheless, the value we obtained is in better agreement with the experimental result for the first compression than for the second (Table 2), indicating that head-on orientation should be the preferred molecular orientation during the BuPTCD film's first compression.

Our predicted value for the surface pressure of the BuPTCD monolayer with head-on orientation at 0.45 nm^2 molecule^{-1} deviates from the experimental isotherm (Table 2). This negative surface pressure indicates the formation of a metastable state that should eventually relax to achieve a small, positive surface pressure, but simulations were not long enough.

In the next section, we shall present structural data characterizing BuPTCD films with the head-on orientation. Although we pointed out that a metastable state was obtained at 0.45 nm^2 molecule^{-1}, the data obtained from this surface area will be presented as well to show the trends in the film ordering as the area changes.

3.2. Molecular Ordering. Besides characterizing which orientation corresponds to each isotherm, molecular dynamics simulations allow a thorough description of the molecular organization for each film. This is an important issue because the degree of order may be correlated with the efficiency of devices using perylene-derivative films (e.g., organic solar cells).[1,2,5−7] Of course, the ordering in a Langmuir film may not be the same as that in a Langmuir−Blodgett film or that in a film obtained with other techniques, but it is certainly a fundamental piece of information in the process of understanding the molecular order in thin films.

The final structures after 1 ns illustrate the fact that BuPTCD films with head-on orientation remained monomolecular as the area changed, whereas some molecules may protrude into water or into the empty space above (Figure 4). It is clear that the molecules are tilted with respect to the interfacial plane. The upper view of the final structures shows that holes may appear in the films as the area per molecule increases, but coverage is almost complete anyway (Figure 5).

The densities of the various systems along the z direction show that BuPTCD protrusion into water is nearly constant in all of the simulations but the film becomes thicker as the surface area decreases (Figure 6). Film thickness was found to depend on BuPTCD's molecular ordering, which may be described in terms of the average spatial orientation of the perylene tetracarboxidiimide moiety. Taking the $N_{14}-N_{51}$ and $C_{25}-C_{29}$ vectors to define a plane for each perylene molecule, the average angles between these two vectors and each reference axis are consistent with a tilted head-on orientation changing to a tilted face-on orientation as the area increases (Figures 7 and 8). It is

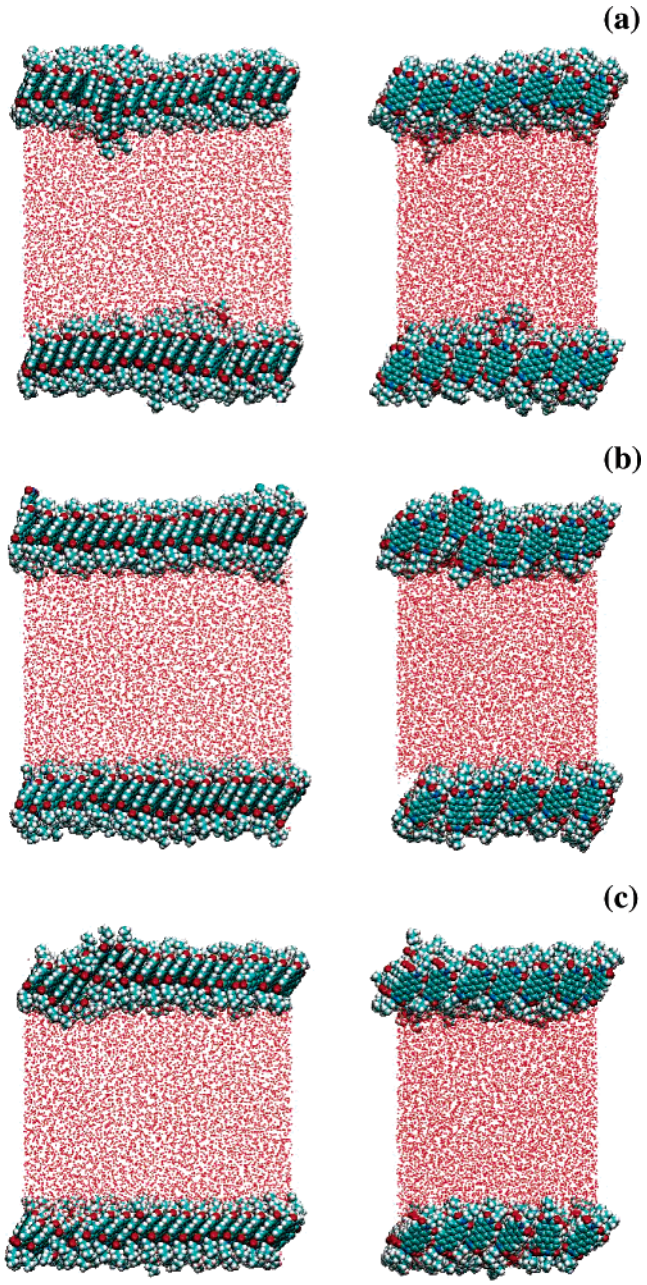

Figure 4. BuPTCD monolayers on water after 1 ns: (a) 0.38 nm^2 $molecule^{-1}$; (b) 0.40 nm^2 $molecule^{-1}$; (c) 0.45 nm^2 $molecule^{-1}$. Carbon atoms are cyan, hydrogen light gray, oxygen red, and nitrogen blue.

clear that the molecules do not align themselves in either a perfect head-on or a perfect face-on orientation. For instance, a perfect face-on orientation would imply that both the $C_{25}-C_{29}$ and $N_{14}-N_{51}$ vectors were perpendicular to the *z* axis regardless of their orientation with respect to the other two reference axes. These requirements are not fulfilled as much as those defining a perfect head-on orientation. Therefore, labels characterizing the perylene orientation in thin films should be used carefully, although edge-on orientation may be ruled out because it would simultaneously imply an average 90° angle between the $C_{25}-C_{29}$ vector and both the *x* and *y* axes, an average 0° angle between this vector and the *z* axis, and an average 90° angle between the $N_{14}-N_{51}$ vector and the *z* axis.

Constantino et al.[43] examined the structures of BuPTCD and three other perylene derivatives on Langmuir−Blodgett films deposited onto glass and glass coated with Ag islands using surface-enhanced fluorescence. The fluorescence spectra suggest that the molecules are arranged tilted head-on in the Langmuir−Blodgett monolayers. Other PTCDs are oriented head-on in Langmuir−Blodgett films as well.[45,46]

The authors of ref 43 also reported a docking calculation of BuPTCD deposition on water that disagreed with both experimental evidences and our simulation results, giving edge-on as the energetically most favorable orientation.[43] The same conclusions were also drawn in a previous work using the docking methodology to study the deposition of four other perylene derivatives.[51]

The results obtained using the docking approach may be reconciled with the structure we found in our molecular-dynamics simulations if we take into account the differences in the sizes of the model systems employed in each case. The docking calculations employed only two perylene molecules and a rigid water slab, resulting in an area per molecule that was 10-fold larger than what we adopted in our simulations. The docking model system is able to correctly describe the BuPTCD/water and BuPTCD/BuPTCD potential-energy profiles in the G phase. During compression, the steric repulsion between BuPTCD molecules will increase, and these repulsive interactions tend to align molecules with their principal axis perpendicular to the water surface, while the dipolar attractive contributions tend to align them parallel to the surface.[17] That explains why the docking-approach results were apparently in disagreement with our molecular dynamics structural picture.

The order parameter (S_z) is related to the average spatial orientation of molecules and may be defined as[47]

$$S_z = \frac{1}{2}\langle 3\cos(\theta_z) - 1\rangle$$

where θ_z is the angle between a reference vector in BuPTCD molecules and the *z* axis and the brackets denote the average over all equivalent atoms and over time. Both the *x* and *y* axes could be used as well, but the perpendicular direction emerges as a natural choice to compute order parameters for monolayers spreading on the $x-y$ plane. S_z values range from -0.5 to $+1.0$, meaning an orientation either fully perpendicular or fully parallel to the *z* axis, respectively. A value of around 0 means an average random orientation of the vector with respect to the *z* axis. For the aliphatic atoms, the line joining the reference atom and the next heavy atom attached to it will define the vectors. For the rings, the line joining the N_{14} and N_{51} atoms will be used as the reference vector.

Two regions inside the BuPTCD molecule may be devised by the S_z values obtained from the simulation: the methyl group and the two methylene groups next to it behave as a liquid hydrocarbon with a low-order parameter, and the methylene groups attached to nitrogen atoms and the perylene rings as a whole are almost as orderly as a liquid crystal (Figure 9). The order parameter did not change upon expansion/compression in the former region, whereas in the latter, the ordering increased as the film was compressed; that is, the change from a tilted face-on to a tilted head-on orientation reported above, which may be pictured as a film-ordering process, concerns only the perylene tetracarboxidiimide moiety because no significant ordering takes place along the tails.

The trend observed for the order parameter of perylene rings was reported for the coarse-grain model lipid, whose overall order parameter was defined taking the head-to-tail vector as a reference.[30] S_z values increased linearly with Langmuir-film surface coverage, reaching ca. 0.9 at 0.61 nm^2 $molecule^{-1}$, consistent with a solid phase. Other simulations of zwitterionic lipids also showed that order parameters increase upon compres-

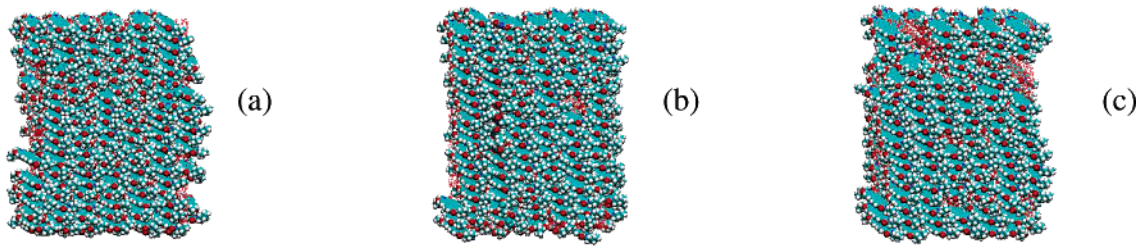

Figure 5. Upper view of the BuPTCD monolayers on water after 1 ns (head-on orientation): (a) 0.38 nm^2 molecule^{-1}; (b) 0.40 nm^2 molecule^{-1}; (c) 0.45 nm^2 molecule^{-1}.

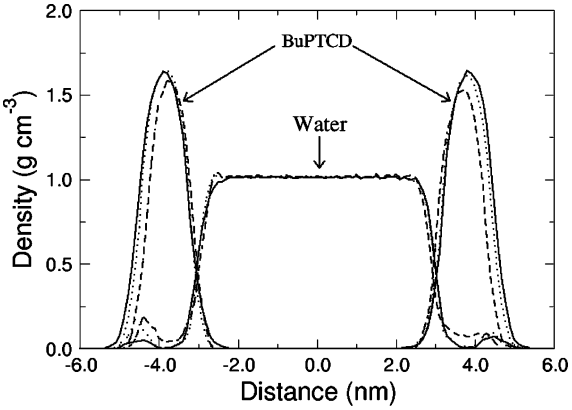

Figure 6. BuPTCD and water-density profile along the *z* direction: (—) 0.38 nm^2 molecule^{-1}; (···) 0.40 nm^2 molecule^{-1}; (- - -) 0.45 nm^2 molecule^{-1}.

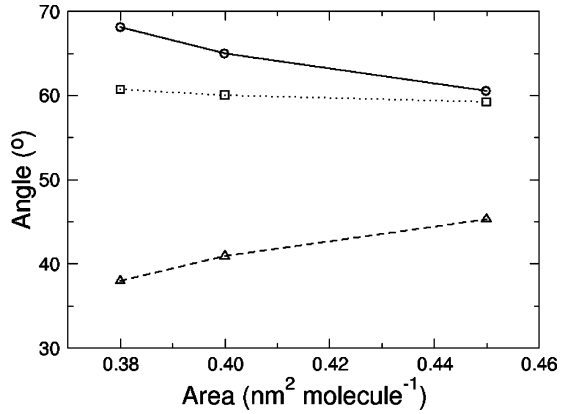

Figure 7. Average angle between the BuPTCD aromatic moiety (N_{14}—N_{51} vector) and reference axes: (—○—) *x* axis; (···□···) *y* axis; (- - -△- - -) *z* axis.

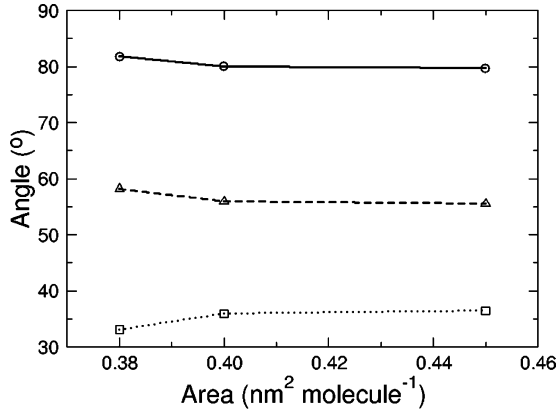

Figure 8. Average angle between the BuPTCD aromatic moiety (C_{25}—C_{29} vector) and reference axes: (—○—) *x* axis; (···□···) *y* axis; (- - -△- - -) *z* axis.

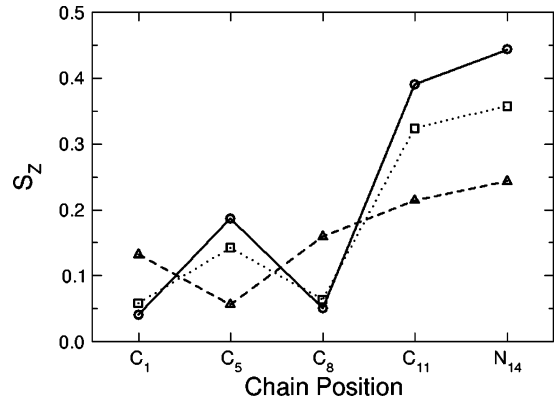

Figure 9. Order parameter of BuPTCD bonds with respect to the *z* axis: (—○—) 0.38 nm^2 molecule^{-1}; (···□···) 0.40 nm^2 molecule^{-1}; (- - -△- - -) 0.45 nm^2 molecule^{-1}.

sion,[27,28] although none of them reported such high values as those derived using the coarse-grain model.

The BuPTCD/water interface may be characterized by means of radial distribution functions, $g_{\alpha\beta}(r)$[47,52]

$$g_{\alpha\beta}(r) = \frac{\rho_{\alpha\beta}(r)}{\rho_{\alpha\beta}}$$

where $\rho_{\alpha\beta}(r)$ is the local density of particles β around reference particles α at a distance r and $\rho_{\alpha\beta}$ is the average density considering the whole system. At short distances, $g_{\alpha\beta}(r)$ becomes zero because repulsive interactions between atoms dominate and preclude molecules to get closer. On the other hand, at large distances, $g_{\alpha\beta}(r)$ approaches unity because attractive interactions can no longer induce any ordering and the density of particles attains its equilibrium value ($g_{\alpha\beta}(r) = 1$ means that the density of particles $\rho_{\alpha\beta}(r)$ becomes uniform and attains its equilibrium value $\rho_{\alpha\beta}$ at large distances). Our simulation box has large evacuated regions above and below the actual system to mimic an air/water interface. This void volume contributes to the average density of particles, thus increasing $g_{\alpha\beta}(r)$ values and requiring the distribution function to be scaled accordingly.

Radial distribution functions give useful structural information at intermediate distances. Molecular ordering arises as a result of the competition between attractive and repulsive interactions that may bring about intricate structural patterns. Correlation peaks indicate the presence of regions where pairs are more likely to be found. Conversely, very low values of a radial-distribution function suggest the existence of regions where the local density may even become null.

Distribution functions may give insight into ordering patterns, but they should be compared with care because the correlation peak intensity varies inversely with the number of reference sites employed to compute these functions. Our model systems had different numbers of BuPTCD molecules within the same interfacial area in order to yield different areas per molecule,

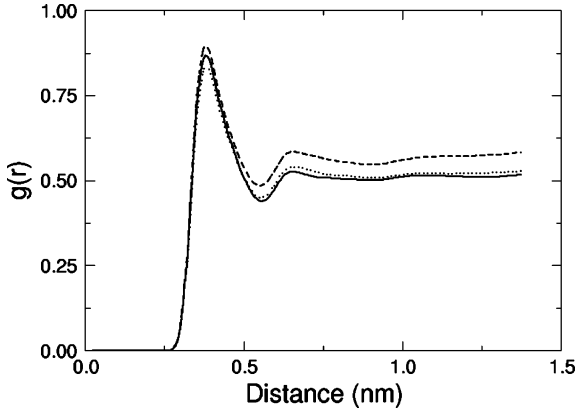

Figure 10. Radial distribution function of water oxygen atoms around BuPTCD C_1/C_{61} atoms: (—) 0.38 nm^2 molecule^{-1}; (···) 0.40 nm^2 molecule^{-1}; (- - -) 0.45 nm^2 molecule^{-1}.

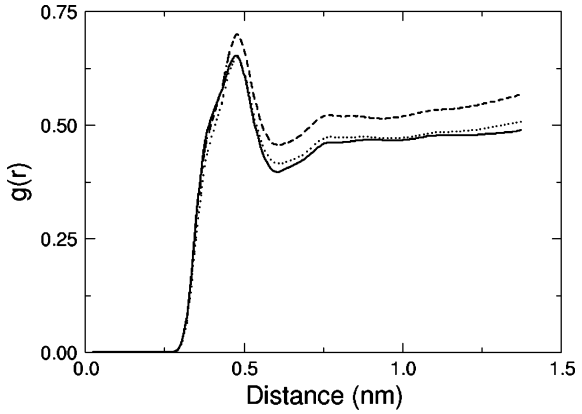

Figure 11. Radial distribution function of water oxygen atoms around BuPTCD C_5/C_{58} atoms: (—) 0.38 nm^2 molecule^{-1}; (···) 0.40 nm^2 molecule^{-1}; (- - -) 0.45 nm^2 molecule^{-1}.

and thus correlation peaks may have increasing heights even if hydration does not change appreciably. A complementary quantity derived from radial distribution functions that may fill out this information gap is the cumulative number ($CN_{\alpha\beta}$) of β atoms around reference α sites

$$CN_{\alpha\beta} = \rho \int_{r_1}^{r_2} 4\pi r^2 g(r)\, dr$$

where $4\pi r^2\, dr$ is the volume element of a spherical shell of radius r and thickness dr around an α reference site. If we regard a correlation peak as a coordination shell, then the integration limits r_1 and r_2 may be chosen in order to obtain average coordination numbers, which are more reliable to describe the relative hydration of any given site than correlation peak heights.

The first thing to note about radial distribution functions of water molecules hydrating BuPTCD is their overall small intensity (Figures 10−15). All correlation functions remained below unity up to the interaction cutoff (1.4 nm); that is, the local density of water molecules at the interfacial region is smaller than the bulk water density. The number of water molecules corresponding to the first correlation peak of each distribution function is rather small along the tails and does not depend on the area per molecule (Figure 16). Even the most hydrated aliphatic group (C_8 methylene group) had only one water molecule for each of five BuPTCD molecules on average. On the other hand, polar sites composing diimide groups had a larger number of water molecules around them, and their hydration increases with the area (Figure 17). We have chosen to present the radial distribution function of water hydrogen

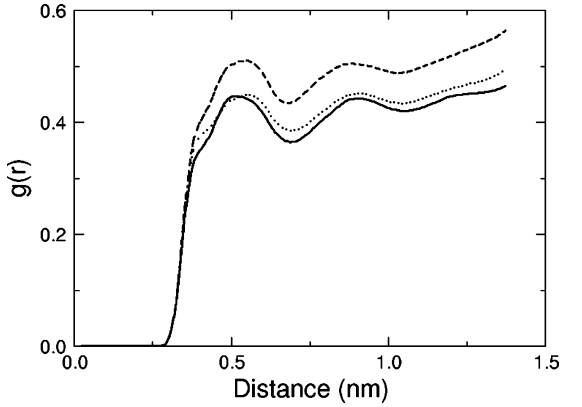

Figure 12. Radial distribution function of water oxygen atoms around BuPTCD C_8/C_{55} atoms: (—) 0.38 nm^2 molecule^{-1}; (···) 0.40 nm^2 molecule^{-1}; (- - -) 0.45 nm^2 molecule^{-1}.

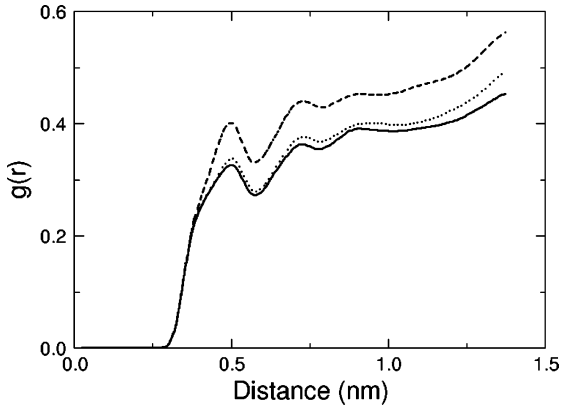

Figure 13. Radial distribution function of water oxygen atoms around BuPTCD C_{11}/C_{52} atoms: (—) 0.38 nm^2 molecule^{-1}; (···) 0.40 nm^2 molecule^{-1}; (- - -) 0.45 nm^2 molecule^{-1}.

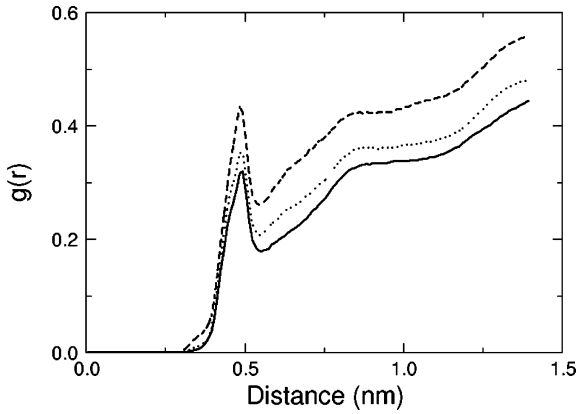

Figure 14. Radial distribution function of water oxygen atoms around BuPTCD nitrogen atoms: (—) 0.38 nm^2 molecule^{-1}; (···) 0.40 nm^2 molecule^{-1}; (- - -) 0.45 nm^2 molecule^{-1}.

atoms around BuPTCD oxygen atoms to emphasize the formation of hydrogen bonds, characterized by a sharp correlation peak around 0.18 nm (Figure 15). The number of hydrogen bonds increases steadily with the area and is 10-fold larger than the hydration numbers of aliphatic-chain atoms (Figure 16). The upper view of BuPTCD monolayers showed that oxygen atoms are exposed to the air above (Figure 5). The same holds true for the oxygen atoms exposed to the water molecules because lateral chains are too short to aggregate and form a barrier between diimide groups and the aqueous subphase. Because water molecules lack specific interactions with the tails, they will preferentially hydrate the hydrophilic oxygen atoms. This

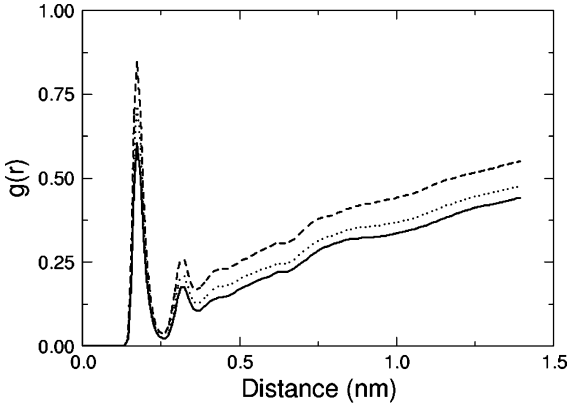

Figure 15. Radial distribution function of water hydrogen atoms around BuPTCD oxygen atoms: (—) 0.38 nm^2 molecule^{-1}; (···) 0.40 nm^2 molecule^{-1}; (- - -) 0.45 nm^2 molecule^{-1}.

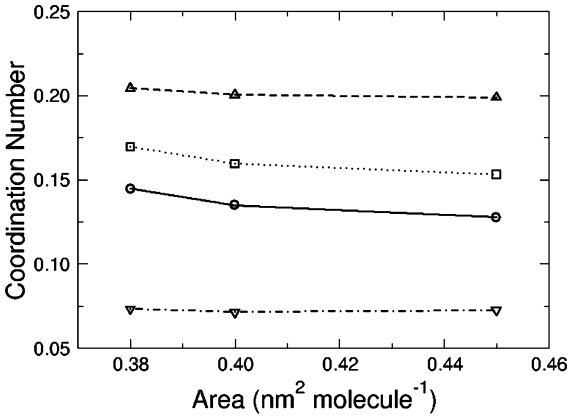

Figure 16. Number of water oxygen atoms in the first coordination shell around BuPTCD apolar atoms: (—○—) C_1/C_{61}; (···□···) C_5/C_{58}; (- - -△- - -) C_8/C_{55}; (-·-▽-·-) C_{11}/C_{52}.

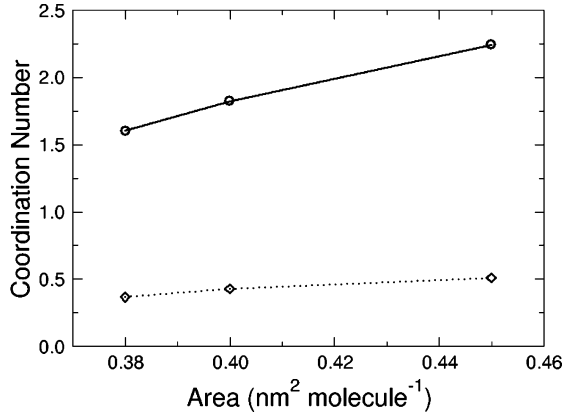

Figure 17. Number of water atoms in the first coordination shell around BuPTCD polar atoms: (—○—) water oxygen atoms around BuPTCD nitrogen atoms; (···◇···) water hydrogen atoms around BuPTCD oxygen atoms.

finding is in agreement with the observations of Kam et al.[53] that water molecules may be trapped into PTCD films by means of hydrogen bonding to the polar moiety and this entrapment induces structural changes in the PTCD films.[53]

The average correlation time of water molecules around BuPTCD atomic sites may be evaluated using the approach devised by Impey et al.[54] We systematically look for water molecules hydrating BuPTCD and follow these pairs along the molecular dynamics trajectory until they break away. The time interval a water molecule remains in the first hydration shell around a reference atomic position is accumulated into a

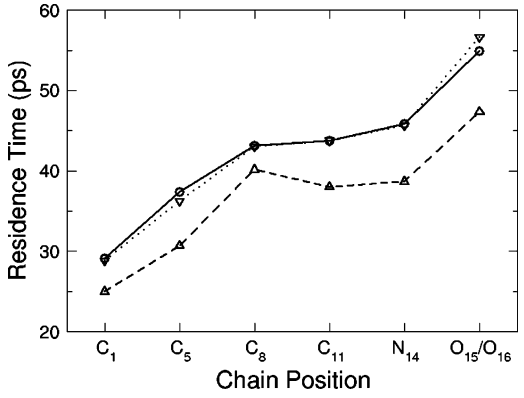

Figure 18. Residence time of water molecules around BuPTCD atoms: (—○—) 0.38 nm^2 molecule^{-1}; (···▽···) 0.40 nm^2 molecule^{-1}; (- - -△- - -) 0.45 nm^2 molecule^{-1}.

histogram, which will be averaged over all of the molecules and all of the time origins to give a time-correlation function. These functions decrease monotonically from 1 to 0, and correlation times may be computed by integrating them. Residence times are nearly equal at 0.38 and 0.40 nm^2 molecule^{-1} but become lower at 0.45 nm^2 molecule^{-1} and increase from the methyl groups to the diimide oxygen atoms for all of the surface areas (Figure 18). Along with the coordination numbers described above, correlation times give an interesting molecular picture of the differences between hydrophilic and hydrophobic regions within a molecule: when compared to hydrophobic atoms, a larger number of water molecules hydrate hydrophilic regions and the solvent molecules stay longer in the first hydration shell of these polar sites.

Structural patterns play an important role in the efficiency of perylene-derivative films in optoelectronic applications.[1−7] Of course, the interactions of PTCD with electromagnetic radiation and charge-transfer processes are essentially quantum mechanical in nature and cannot be adequately described by classical molecular dynamics simulations. Notwithstanding that, we may evaluate the electric potential profile across the interfacial region and the way it changes in response to the monolayer structure. The electric potential in the *z* direction may be derived from the molecular dynamics trajectory by double integrating the charge density $\rho(z)$[47]

$$\psi(z) - \psi(\infty) = \frac{1}{\epsilon}\int_{-\infty}^{z} dz' \int_{-\infty}^{z'} \rho(z'')\, dz''$$

where ϵ is the electric permittivity, usually considered to be the vacuum permittivity, ϵ_0, and the electric potential at infinity is set to 0. The electric potential profile across the system presents a positive barrier on each organic monolayer and a deep negative well on water (Figure 19). The heights of the potential barriers changed appreciably with the area per molecule, indicating that the electric properties of PTCD films are likely to depend on the molecular ordering.

4. Conclusions

The results obtained from our molecular dynamics simulations allowed a detailed description of the structures of BuPTCD Langmuir films. Geometrical reasoning and surface pressure showed that perylene molecules must be oriented mainly head-on toward the water surface. The average orientation of the perylene tetracarboxidiimide moiety during simulations ruled out the edge-on orientation and indicated that molecular alignment is not simple, changing from tilted face-on to tilted head-on during compression. Films become more orderly at a

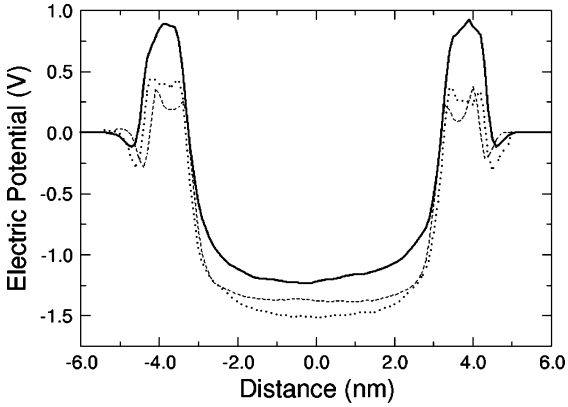

Figure 19. Electric potential along the *z* direction: (—) 0.38 nm^2 molecule^{-1}; (•••) 0.40 nm^2 molecule^{-1}; (- - -) 0.45 nm^2 molecule^{-1}.

small surface area, mostly at the rigid perylene core. The change in orientation resulted in the thickening of the BuPTCD film as the area decreased. BuPTCD had few solvent molecules hydrating the hydrophobic tails, whereas a considerable number of them were hydrogen bonded to diimide oxygen atoms. Besides, the residence times of water molecules around perylene atomic sites increased from the terminal methyl groups to the diimide oxygen atoms. Finally, the electric potential across the monolayer was found to depend on the area occupied by each molecule, with a considerable change of the potential barrier height due to the monolayer structure.

The present work showed that atomistic simulations of large molecular assemblies have become feasible and a wealth of detailed information may be derived from molecular dynamics trajectories. It will be necessary to carry out quantum chemical calculations on BuPTCD clusters to further understand how the molecular ordering affects electronic structure, unraveling significant aspects of the efficiency of organic solar cells and other related devices.

Acknowledgment. The authors thank CNPq and FAPESP (Brazilian funding agencies) for financial support. A.F.M. also thanks FAPESP for the award of a postdoctoral fellowship (Grant 04/00124-2).

References and Notes

(1) Wöhrle, D.; Kreienhoop, L.; Schnurpfeil, G.; Elbe, J.; Tennigkeit, B.; Hiller, S.; Schlettwein, D. Investigations of n/p-Junction Photovoltaic Cells of Perylenetetracarboxylic Acid Diimides and Phthalocyanines. *J. Mater. Chem.* **1995**, *5*, 1819−1829.

(2) Peumans, P.; Bulović, V.; Forrest, S. R. Efficient Photon Harvesting at High Optical Intensities in Ultrathin Organic Double-Heterostructure Photovoltaic Diodes. *Appl. Phys. Lett.* **2000**, *76*, 2650−2652.

(3) Kavassalis, T. A.; Kazmaier, P. M.; Bareman, J. P.; Sundararajan, P. R.; Wright, J. D. Computational Chemistry and the Design of New Materials for Xerographic Applications. *Ind. Eng. Chem. Res.* **1995**, *34*, 4174−4184.

(4) Ivri, J.; Burshtein, Z.; Miron, E.; Reisfeld, R.; Eyal, M. The Perylene Derivative BASF-241 Solution as a New Tunable Dye Laser in the Visible. *IEEE J. Quantum Electron.* **1990**, *26*, 1516−1520.

(5) Gregg, B. A. Evolution of Photophysical and Photovoltaic Properties of Perylene Bis(phenethylimide) Films upon Solvent Vapor Annealing. *J. Phys. Chem.* **1996**, *100*, 852−859.

(6) Cormier, R. A.; Gregg, B. A. Self-Organization in Thin Films of Liquid Crystalline Perylene Diimides. *J. Phys. Chem. B* **1997**, *101*, 11004−11006.

(7) Gregg, B. A.; Sprague, J.; Peterson, M. W. Long-Range Singlet Energy Transfer in Perylene Bis(phenethylimide) Films. *J. Phys. Chem. B* **1997**, *101*, 5362−5369.

(8) Mercadante, R.; Trsic, M.; Duff, J.; Aroca, R. Molecular Orbital Calculations of Perylene Tetracarboxilic Monoimide and Bisimide. Alkyl Derivatives and Hetero Atom Analogues. *THEOCHEM* **1997**, *349*, 215−226.

(9) Hädicke, E.; Graser, F. Structures of 11 Perylene-3,4-9,10-bis-(Dicarboximide) Pigments. *Acta Crystallogr., Sect. C: Cryst. Struct. Commun.* **1986**, *42*, 189−195.

(10) Hädicke, E.; Graser, F. Structures of 3 Perylene-3,4-9, 10-bis-(Dicarboximide) Pigments. *Acta Crystallogr., Sect. C* **1986**, *42*, 195−198.

(11) Klebe, G.; Graser, F.; Hädicke, E.; Berndt, J. Crystallochromy as a Solid-State Effect−Correlation of Molecular-Conformation, Crystal Packing and Color in Perylene-3,4-9,10-bis(Dicarboximide) Pigments. *Acta Crystallogr., Sect. B* **1989**, *45*, 69−77.

(12) Mizugushi, J. Crystal Structure of a Second Modification of N,N′-di-*n*-Butilperylene-3,4:9,10-bis(Dicarboximide), $C_{32}H_{26}N_2O_4$. *Z. Kristallogr.* **2003**, *218*, 131−133.

(13) Kazmaier, P. M.; Hoffmann, R. A Theoretical Study of Crystallochromy. Quantum Interference Effects in the Spectra of Perylene Pigments. *J. Am. Chem. Soc.* **1994**, *116*, 9684−9691.

(14) Liu, S. G.; Sui, G. D.; Cormier, R. A.; Leblanc, R. M.; Gregg, B. A. Self-Organizing Liquid Crystal Perylene Diimide Thin Films: Spectroscopy, Crystallinity, and Molecular Orientation. *J. Phys. Chem. B* **2002**, *106*, 1307−1315.

(15) Adamson, A. W. *Physical Chemistry of Surfaces*, 5th ed.; Wiley-Interscience Publication: New York, 1990.

(16) Dynarowicz-Latka, P.; Dhanabalan, A.; Oliveira, O. N., Jr. Modern Physicochemical Research on Langmuir Monolayers. *Adv. Colloid Interface Sci.* **2001**, *91*, 221−293.

(17) Iwamoto, M.; Wu, C.-X.; Zhong-can, O.-Y. Tilting Phase Transition of Langmuir Monolayers: a Competition Between Steric Repulsion and Interaction of Dipolar Molecules with Liquid Surface. *Chem. Phys. Lett.* **1999**, *312*, 7−13.

(18) Collazo, N.; Shin, S.; Rice, S. A. Molecular-Dynamics Studies of the Structure and Properties of Monolayers of Perfluorinated Amphiphiles. *J. Chem. Phys.* **1992**, *96*, 4735−4742.

(19) Karaborni, S.; Toxvaerd, S. Molecular Dynamics Simulations of Langmuir Monolayers: A Study of Structure and Thermodynamics. *J. Chem. Phys.* **1992**, *96*, 5505−5515.

(20) Karaborni, S. Molecular Dynamics Simulations of Long-Chain Amphiphilic Molecules in Langmuir Monolayers. *Langmuir* **1993**, *9*, 1334−1343.

(21) Siepman, J. I.; Karaborni, S.; Klein, M. L. Monte Carlo Simulation of the Liquid−Vapor Coexistence in a Langmuir Monolayer of Pentadecanoic Acid. *J. Phys. Chem.* **1994**, *98*, 6675−6678.

(22) Ahlström, P.; Berendsen, H. J. C. A Molecular Dynamics Study of Lecithin Monolayers. *J. Phys. Chem.* **1993**, *97*, 13691−13702.

(23) van Buuren, A. R.; Marrink, S. J.; Berendsen, H. J. C. Characterisation of Aqueous Interfaces with Different Hydrophobicities by Molecular Dynamics. *Colloids Surf., A* **1995**, *102*, 143−157.

(24) Okamura, E.; Fukushima, N.; Hayashi, S. Molecular Dynamics Simulation of the Vibrational Spectra of Stearic Acid Monolayers at the Air/Water Interface. *Langmuir* **1999**, *15*, 3589−3594.

(25) Shelley, M. Y.; Sprik, M.; Shelley, J. C. Pattern Formation in a Self-Assembled Soap Monolayer on the Surface of Water: A Computer Simulation Study. *Langmuir* **2000**, *16*, 626−630.

(26) Dhathathreyan, A.; Collins, S. J. Molecular Dynamics Simulation of (Octadecylamino)dihydroxysalicylaldehyde at Air/Water Interface. *Langmuir* **2002**, *18*, 928−931.

(27) Feller, S. E.; Zhang, Y.; Pastor, R. W. Computer Simulation of Liquid/Liquid Interfaces. II. Surface Tension-Area Dependence of a Bilayer and Monolayer. *J. Chem. Phys.* **1995**, *103*, 10267−10276.

(28) Kaznessis, Y. N.; Kim, S.; Larson, R. G. Simulations of Zwitterionic and Anionic Phospholipid Monolayers. *Biophys. J.* **2002**, *82*, 1731−1742.

(29) Sun, F. Constant Normal Pressure, Constant Surface Tension, and Constant Temperature Molecular Dynamics Simulation of Hydrated 1,2-Dilignoceroylphosphatidylcholine Monolayer. *Biophys. J.* **2002**, *82*, 2511−2519.

(30) Nielsen, S. O.; Lopez, C. F.; Moore, P. B.; Shelley, J. C.; Klein, M. L. Molecular Dynamics Investigations of Lipid Langmuir Monolayers Using a Coarse-Grain Model. *J. Phys. Chem. B* **2003**, *107*, 13911−13917.

(31) Tieleman, D. P.; Marrink, S. J.; Berendsen, H. J. C. A Computer Perspective of Membranes: Molecular Dynamics Studies of Lipid Bilayer Systems. *Biochim. Biophys. Acta* **1997**, *1331*, 235−270.

(32) Shinoda, W.; Namiki, N.; Ozaki, S. Molecular Dynamics Study of a Lipid Bilayer: Convergence, Structure, and Long-Time Dynamics. *J. Chem. Phys.* **1997**, *106*, 5731−5743.

(33) Paci, E.; Marchi, M. Constant-Pressure Molecular Dynamics Techniques Applied to Complex Molecular Systems and Solvated Proteins. *J. Phys. Chem.* **1996**, *100*, 4314−4322.

(34) Maillet, J.-B.; Lachet, V.; Coveney, P. V. Large Scale Molecular Dynamics Simulation of Self-Assembly Processes in Short and Long Chain Cationic Surfactants. *Phys. Chem. Chem. Phys.* **1999**, *1*, 5277−5290.

(35) Marrink, S. J.; Tieleman, D. P.; Mark, A. E. Molecular Dynamics of the Kinetics of Spontaneous Micelle Formation. *J. Phys. Chem. B* **2000**, *104*, 12165−12173.

(36) Marrink, S. J.; Lindahl, E.; Edholm, O.; Mark, A. E. Simulation of the Spontaneous Aggregation of Phospholids into Bilayers. *J. Am. Chem. Soc.* **2001**, *123*, 8638−8639.

(37) Berendsen, H. J. C.; Postma, J. P. M.; van Gunsteren, W. F.; Hermans, J. In *Intermolecular Forces*; Pullman, B., Ed.; Reidel: Dordrecht, The Netherlands, 1981.

(38) Jorgensen, W. L.; Maxwell, D. S.; Tirado-Rives, J. Development and Testing of the OPLS All-Atoms Force Field on Conformational Energetics and Properties of Organic Liquids. *J. Am. Chem. Soc.* **1996**, *118*, 11225−11236.

(39) Bayly, C. I.; Cieplak, P.; Cornell, W. D.; Kollman, P. A. A Well-Behaved Electrostatic Potential Based Method Using Charge Restraints for Determining Atom-Centered Charges: The RESP Model. *J. Phys. Chem.* **1993**, *97*, 10269.

(40) Cornell, W. D.; Cieplak, P.; Bayly, C. I.; Kollman, P. A. Application of RESP Charges to Calculate Conformational Energies, Hydrogen Bond Energies, and Free Energies of Solvation. *J. Am. Chem. Soc.* **1993**, *115*, 9620.

(41) Frisch, M. J.; Trucks, G. W.; Schlegel, H. B.; Scuseria, G. E.; Robb, M. A.; Cheeseman, J. R.; Montgomery, J. A., Jr.; Vreven, T.; Kudin, K. N.; Burant, J. C.; Millam, J. M.; Iyengar, S. S.; Tomasi, J.; Barone, V.; Mennucci, B.; Cossi, M.; Scalmani, G.; Rega, N.; Petersson, G. A.; Nakatsuji, H.; Hada, M.; Ehara, M.; Toyota, K.; Fukuda, R.; Hasegawa, J.; Ishida, M.; Nakajima, T.; Honda, Y.; Kitao, O.; Nakai, H.; Klene, M.; Li, X.; Knox, J. E.; Hratchian, H. P.; Cross, J. B.; Adamo, C.; Jaramillo, J.; Gomperts, R.; Stratmann, R. E.; Yazyev, O.; Austin, A. J.; Cammi, R.; Pomelli, C.; Ochterski, J. W.; Ayala, P. Y.; Morokuma, K.; Voth, G. A.; Salvador, P.; Dannenberg, J. J.; Zakrzewski, V. G.; Dapprich, S.; Daniels, A. D.; Strain, M. C.; Farkas, O.; Malick, D. K.; Rabuck, A. D.; Raghavachari, K.; Foresman, J. B.; Ortiz, J. V.; Cui, Q.; Baboul, A. G.; Clifford, S.; Cioslowski, J.; Stefanov, B. B.; Liu, G.; Liashenko, A.; Piskorz, P.; Komaromi, I.; Martin, R. L.; Fox, D. J.; Keith, T.; Al-Laham, M. A.; Peng, C. Y.; Nanayakkara, A.; Challacombe, M.; Gill, P. M. W.; Johnson, B.; Chen, W.; Wong, M. W.; Gonzalez, C.; Pople, J. A. *Gaussian 03*, revision B.04; Gaussian, Inc.: Pittsburgh, PA, 2003.

(42) Pigache, A.; Cieplak, P.; Dupradeau, F.-Y. Automatic and Highly Reproducible RESP and ESP Charge Derivation: Application to the Development of Programs RED and X RED. ACS National Meeting, Anaheim, CA, March 28−April 1, 2004.

(43) Constantino, C. J. L.; Antunes, P. A.; Oliveira, C. B.; Trsic, M.; Caracelli, I.; Aroca, R. F. Surface Pressure-Area Isotherms for Langmuir Monolayers and a Docking Molecular Orientation of Perylene Tetracarboxilic Derivatives on a Water Surface. *Can. J. Anal. Sci. Spectrosc.* **2004**, *49*, 64−72.

(44) de Moura, A. F.; Freitas, L. C. G. Molecular Dynamics Simulation of the Sodium Octanoate Micelle in Aqueous Solution: Comparison of Force Field Parameters and Molecular Topology Effects on the Micellar Structure. *Braz. J. Phys.* **2004**, *34*, 64−72.

(45) Antunes, P. A.; Constantino, C. J. L.; Aroca, R. F.; Duff, J. Langmuir and Langmuir−Blodgett Films of Perylene Tetracarboxylic Derivatives with Varying Alkyl Chain Length: Film Packing and Surface-Enhanced Fluorescence Studies. *Langmuir* **2001**, *17*, 2958−2964.

(46) del Caño, T.; Parra, V.; Rodriguez-Mendez, M. L.; Aroca, R.; de Saja, J. A. Molecular Stacking and Emission Properties in Langmuir−Blodgett Films of Two Alkyl Substituted Perylene Tetracarboxylic Diimides. *Org. Electron.* **2004**, *5*, 107−114.

(47) van der Spoel, D.; Lindahl, E.; Hess, B.; van Buuren, A. R.; Apol, E.; Meulenhoff, P. J.; Tieleman, D. P.; Sijbers, A. L. T. M.; Feenstra, K. A.; van Drunen, R.; Berendsen, H. J. C. *Gromacs User Manual*, version 3.2. http://www.gromacs.org (2004).

(48) Berendsen, H. J. C.; Postma, J. P. M.; DiNola, A.; Haak, J. R. Molecular Dynamics with Coupling to an External Bath. *J. Chem. Phys.* **1984**, *81*, 3684−3690.

(49) Lindahl, E.; Hess, B.; van der Spoel, D. GROMACS 3.0: A Package for Molecular Simulation and Trajectory Analysis. *J. Mol. Model.* **2001**, *7*, 306−317.

(50) Berendsen, H. J. C.; van der Spoel, D.; van Drunen, R. GROMACS: A Message-Passing Parallel Molecular Dynamics Implementation. *Comput. Phys. Commun.* **1995**, *91*, 43−56.

(51) Oliveira, C. B.; Caracelli, I.; Trsic, M. A Docking Approach for the Deposition of Perylene Derivatives on a Water Surface. *Mater. Chem. Phys.* **2003**, *80*, 457−460.

(52) Allen, M. P.; Tildesley, D. J. *Computer Simulation of Liquids*, 1st ed.; Clarendon Press: Oxford, U.K., 1987.

(53) Kam, A. P.; Aroca, R.; Duff, J.; Tripp, C. P. Role of Water in the Molecular Reorientation of Thermal Annealing of Bis(*n*-propylimido)-Perylene Films. *Langmuir* **2000**, *16*, 1185−1188.

(54) Impey, R. W.; Madden, P. A.; McDonald, I. R. Hydration and Mobility of Ions in Solution. *J. Phys. Chem.* **1983**, *87*, 5071−5083.